AGU PUBLICATIONS

Space Weather

RESEARCH ARTICLE
10.1002/2014SW001130

Key Points:
- Tomographic inner-boundaries are used to drive ENLIL in real-time
- CMEs, shocks, and other interplanetary structures are predicted
- Several comparisons and a successful prediction are shown

Correspondence to:
B. V. Jackson,
bvjackson@ucsd.edu

Citation:
Jackson, B. V., et al. (2015), The UCSD kinematic IPS solar wind boundary and its use in the ENLIL 3-D MHD prediction model, *Space Weather*, *13*, 104–115, doi:10.1002/2014SW001130.

Received 3 OCT 2014
Accepted 8 JAN 2015
Accepted article online 10 JAN 2015
Published online 5 FEB 2015

The UCSD kinematic IPS solar wind boundary and its use in the ENLIL 3-D MHD prediction model

B. V. Jackson[1], D. Odstrcil[2,3], H.-S. Yu[1], P. P. Hick[1], A. Buffington[1], J. C. Mejia-Ambriz[1,4], J. Kim[5], S. Hong[5], Y. Kim[5], J. Han[5], and M. Tokumaru[6]

[1]Center for Astrophysics and Space Sciences, University of California, San Diego, La Jolla, California, USA, [2]School of Physics, Astronomy, and Computational Sciences, George Mason University, Fairfax, Virginia, USA, [3]NASA GSFC, Greenbelt, Maryland, USA, [4]SCiESMEX, Instituto de Geofisica, Unidad Michoacan, Universidad Nacional Autonoma de Mexico, Morelia, Mexico, [5]Korean Space Weather Center, National Radio Research Agency, Jeju-si, South Korea, [6]Solar-Terrestrial Environment Laboratory, Nagoya University, Chikusa-ku, Japan

Abstract The University of California, San Diego interplanetary scintillation (IPS) time-dependent kinematic 3-D reconstruction technique has been used and expanded upon for over a decade to provide predictions of heliospheric solar wind parameters. These parameters include global reconstructions of velocity, density, and (through potential field modeling and extrapolation upward from the solar surface) radial and tangential interplanetary magnetic fields. Time-dependent results can be extracted at any solar distance within the reconstructed volume and are now being exploited as inner boundary values to drive the ENLIL 3-D MHD model in near real time. The advantage of this coupled system is that it uses the more complete physics of 3-D MHD modeling to provide an automatic prediction of coronal mass ejections and solar wind stream structures several days prior to their arrival at Earth without employing coronagraph observations. Here we explore, with several examples, the current differences between the IPS real-time kinematic analyses and those from the ENLIL 3-D MHD modeling using IPS-derived real-time boundaries. Future possibilities for this system include incorporating many different worldwide IPS stations as input to the remote sensing analysis using ENLIL as a kernel in the iterative 3-D reconstructions.

1. Introduction

Heliospheric remote sensing from interplanetary scintillation (IPS) using meter-wavelength intensity variations from point radio sources (pulsars, quasi-stellar objects) has had a long development period [e.g., *Hewish et al.*, 1964; *Ananthakrishnan et al.*, 1980; *Tokumaru*, 2013]. Observations of these small-scale (~150 km) density variations along the line of sight (LOS) are typically available from a few to up to several hundreds of radio sources over a wide range of solar elongations (angular distances from the Sun). Using the Cambridge IPS array in the UK, *Houminer* [1971] was one of the first to view heliospheric structures that can be classified as either corotating or detached from the Sun [*Gapper et al.*, 1982; *Hewish and Bravo*, 1986; *Behannon et al.*, 1991]. Because remotely sensed IPS observations can view heliospheric features at intermediate distances between the Sun and the Earth, these analyses have often been used in predictive models of the Earth arrival of heliospheric structures. These analyses have been promoted at solar-terrestrial forecast centers because of their potential to indicate geomagnetic changes. Since 1999, routine observations at the Solar-Terrestrial Environment Laboratory (STELab), Japan, have been used for space weather predictions [*Jackson et al.*, 2011; *Tokumaru*, 2013].

1.1. The IPS Analysis and Time-Dependent Reconstructions

To optimize the use of IPS observations and produce three-dimensional (3-D) global heliospheric representations, the University of California, San Diego (UCSD) and STELab heliospheric groups have separately developed iterative Computer Assisted Tomography (CAT) programs [*Kojima et al.*, 1998; *Jackson et al.*, 1998, 2003; *Jackson and Hick*, 2005] that fit IPS observations of velocity perpendicular to the line of sight and scintillation level to a kinematic solar wind model to provide velocities and densities. For mathematical details about the UCSD CAT program, see *Hick and Jackson* [2004] and *Jackson et al.* [2008]. These 3-D reconstruction programs fit IPS data from STELab (Figure 1) [*Kojima and Kakinuma*, 1987; *Kojima et al.*, 2002; *Tokumaru et al.*, 2011] and have permitted the development and operation of a near real-time prediction analysis system [*Jackson and Hick*, 2005; *Jackson*

10.1002/2014SW001130

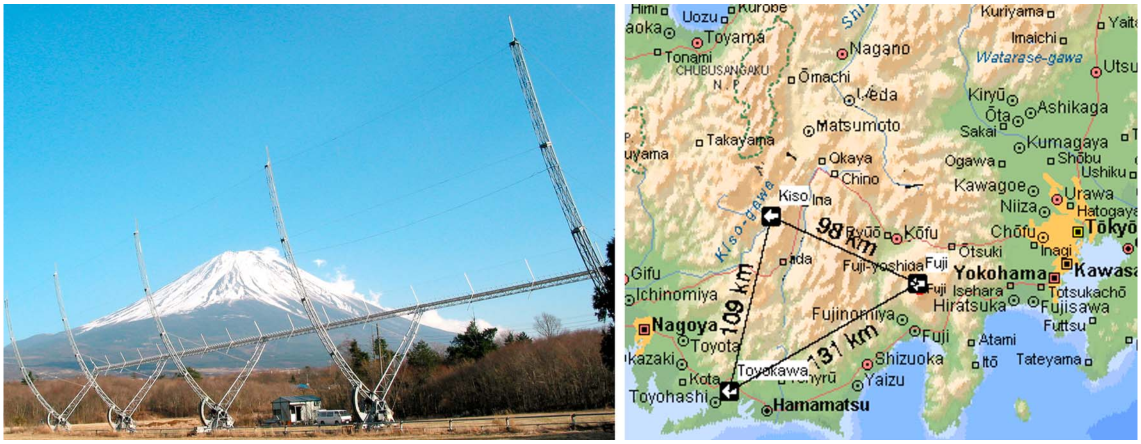

(a) (b)

Figure 1. (a) The Solar-Terrestrial Environment Laboratory (STELab), Japan, radio array near Mount Fuji. (b) Locations and the baseline lengths between the STELab IPS array sites that are used in the present real-time IPS analysis.

et al., 2010a, 2012, 2013], since the time-dependent technique was developed in 1999. In these analyses, IPS results are compared with velocities measured in near real time from the Advanced Composition Explorer (ACE) spacecraft [*Stone et al.*, 1998] Solar Wind Electron Proton Alpha Monitor [*McComas et al.*, 1998] and densities measured from ACE or from the Charge, ELement and Isotope Analysis System (CELIAS) proton monitor [*Hovestadt et al.*, 1995] on board the Solar and Heliospheric Observatory (SOHO) spacecraft [*Domingo et al.*, 1995]. These analyses, with updates in near real time, are available on websites at UCSD http://ips.ucsd.edu, the NASA Goddard Community Coordinated Modeling Center http://iswa.ccmc.gsfc.nasa.gov [*MacNeice et al.*, 2011; *MacNeice*, 2012], and the Korean Space Weather Center (KSWC) http://www.spaceweather.go.kr/models/ips [*Kim and No*, 2013].

Figure 2 is an example of the near real-time UCSD IPS prediction analysis as presented on the KSWC website. Because speeds remain generally constant within a factor of 2 in the heliosphere, and material expands outward as a spherical shell, the ecliptic cut through the reconstructed density in Figure 2 has a 1 AU normalized r^{-2} falloff removed to better display same structure from near to far from the Sun as it moves outward. In these prediction analyses, the in situ comparison continues through the time that in situ densities are available and beyond this, to predict future values. In situ ACE densities and velocities are usually smoothed in time with a 1 day moving mean to make them commensurate with the low-resolution IPS 3-D reconstruction analysis as in Figure 2. This analysis has been operated using STELab data at UCSD since the year 2000 and at KSWC since spring 2013.

Other radio arrays dedicated to the exclusive observation of IPS signals have a long history of operation including the 327 MHz Ootacamund (Ooty), India, radio array [*Manoharan*, 2010], and the 111 MHz Big Scanning Array (BSA) in Pushchino, Russia [*Chashei et al.*, 2013], but currently, these do not have real-time data access. Recently, two more radio arrays are undergoing tests, with the intent to join this group and in providing real-time internet access to their data; the 327 MHz array at KSWC, Jeju, South Korea [*Kim and No*, 2013], and the 140 MHz Mexican Array Radio Telescope (MEXART) near Morelia, Mexico [*Mejia-Ambriz et al.*, 2010; J. C. Mejia-Ambriz et al., Observations of Interplanetary Scintillation (IPS) Using the Mexican Array Telescope (MEXART), submitted to *Solar Physics*, 2014].

The UCSD 3-D reconstruction uses a time cadence interval (usually 1 day for STELab data) short compared with that of a solar rotation. This short interval enables the reconstructions to use outward solar wind motion and the varying LOS weighting to provide perspective views of heliospheric structures as they move outward from the Sun [*Jackson and Hick*, 2005; *Jackson et al.*, 2011, and references therein]. Spatial and temporal resolutions from this technique are limited by the current low-resolution IPS observational coverage and signal-to-noise of each radio source observed.

The UCSD 3-D reconstruction of velocities and densities at Earth [e.g., *Jackson et al.*, 2003; *Jackson and Hick*, 2005; *Bisi et al.*, 2007, 2008, 2009] and at Mars [*Jackson et al.*, 2007] have performed well in retrospective analyses. Real-time IPS predictions often suffer reduced performance since they are limited to the data available only up to the time the prediction is made. A more complete analysis results when the

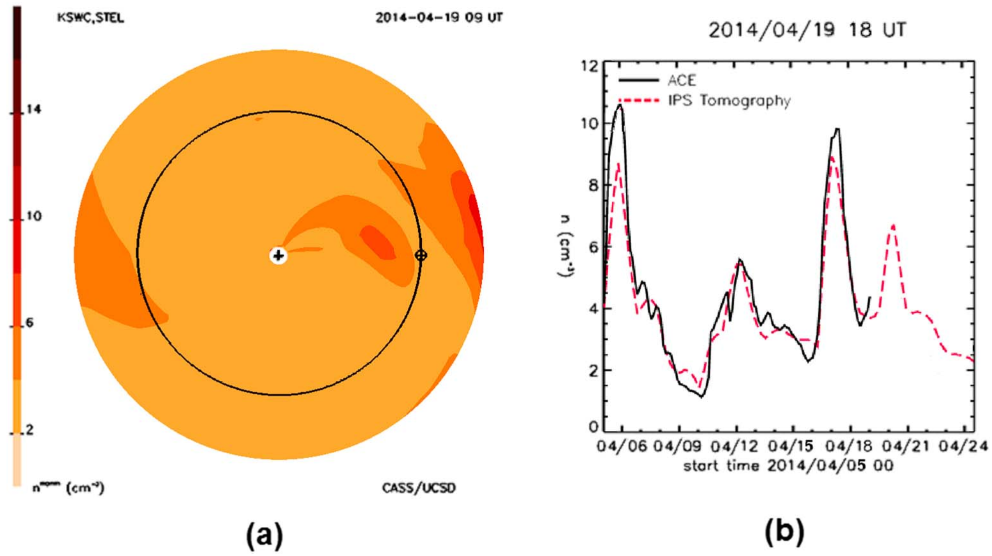

Figure 2. (a) Near real-time ecliptic cut from the UCSD 3-D reconstruction analysis as presented at the KSWC on 19 April 2014. The Sun is at the center of the ecliptic cut, and the Earth is to its right, shown together with its 1 AU orbit. (b) In situ comparison of the ACE proton density data at L_1/Earth with the IPS 3-D reconstructed density; predicted values are from 03:00 UT on 19 April to 24 April where no in situ data are plotted.

heliospheric features first viewed close to the Sun are then followed until they pass beyond the edge of the reconstructed volume near 3 AU. In this case, information along each LOS is completely determined throughout the whole period of observation. An extension to the UCSD tomographic analysis developed more recently [*Jackson et al.*, 2010a, 2013] incorporates in situ velocity and density measurements at Earth at the appropriate spatial and temporal resolutions of the 3-D reconstructions into the iterated results. As expected, this significantly refines predictions at Earth, since each LOS extending outward better matches the measurements that one is trying to reproduce at Earth and blends the in situ result into the one remotely sensed by the IPS.

The 3-D reconstruction of the solar wind velocity is used to forward model the current sheet source surface magnetic field model developed by *Zhao and Hoeksema* [1995], extending it out to the edge of the global boundary considered by this IPS analysis. More detailed descriptions of this are found in *Dunn et al.* [2005] and in *Jackson et al.* [2012]. Direct measurements of rapidly varying transient coronal mass ejection (CME) magnetic fields in the corona and inner heliosphere are essentially unavailable, and usually only the general background fields are mapped outward from the Sun, especially for real-time predictions. This is true of both the UCSD kinematic modeling and the IPS-driven ENLIL (see following sections) analysis that often uses Wang-Sheeley-Arge-derived (WSA) *Arge and Pizzo*, 2000] parameter inputs.

1.2. The 3-D MHD Heliospheric Modeling Effort Specific to the Present IPS Analysis

Numerical solar wind models based on magnetohydrodynamic (MHD) equations are currently the only self-consistent method capable of bridging the large heliospheric distances from near the Sun to well beyond the Earth's orbit. Although MHD is only an approximation to actual plasma behavior, these models have successfully simulated many important space-plasma processes. STELab currently operates a 3-D MHD predictive model as mentioned briefly by *Shibata and Kamide* [2007] using corotating IPS inputs updated on a daily basis, and these also include magnetic field inputs [*Hayashi et al.*, 2003; *Hayashi*, 2012] from the Solar Dynamics Observatory Helioseismic and Magnetic Imager [*Scherrer et al.*, 2012] on their website at http://stsw1.stelab.nagoya-u.ac.jp/mhdtomo/daily_ips_main.html.

Recently, many groups making 3-D MHD calculations have been interested in incorporating our IPS boundaries to drive their models. These groups include (1) the University of Alabama, Huntsville [*Kim et al.*, 2012, 2014; *Yu et al.*, 2012, 2013] with the Multi-Scale FLUid-Kinetic Simulation Suite; (2) the Naval Research Laboratory, with a model termed H3D MHD [*Wu et al.*, 2007; *Yu et al.*, 2013]; and (3) the University of Michigan with the Block Adaptive Tree Solar-wind Roe Upwind Scheme MHD model also employing the coupled solar corona and inner heliosphere components of the Space Weather Modeling Framework [*Toth et al.*, 2012; *Meng*, 2013]. In addition, we continue a long-term association with (4) the ENLIL 3-D MHD model [*Odstrcil*, 2003; *Odstrcil et al.*, 2005, 2007, 2008; *Jackson et al.*, 2010b], which is used extensively in this article.

ENLIL (named after the Sumerian “God of Wind”) is based on an ideal 3-D MHD description, plus two continuity equations to track injected CME material and the magnetic field polarity [see *Odstrcil and Pizzo*, 1999]. Coronal and heliospheric MHD modeling generally employs photospheric magnetic field observations and approximates plasma parameters (velocity, density, and temperature) as boundary conditions at the base of the heliosphere and extrapolates these outward. Some of these parameters, such as velocity and density, are difficult to extract from near-Sun observations for transient events: these are either approximations based on analytic and empirical models to the 3-D sources of energy that eject plasma from the Sun or fit to coronagraph data for outward speeds of fast-moving transient structures.

In contrast, the kinematic solar wind model used as a kernel in our 3-D reconstruction simply conserves mass and mass flux with solar distance assuming radial outward expansion. Even though ENLIL incorporates more advanced physical principles, this simple kinematic model has proven adequate to determine the morphology, outward Sun-Earth propagation, and general 3-D global location of heliospheric velocity and density structures using the low-resolution STELab IPS data. As a further benefit, the kinematic model runs very quickly on present-day single-core PC processors, completing 18 iterations for a monthlong period of data in fewer than 5 min.

An appropriate next step is a hybrid model that couples the two systems into a low-resolution prediction analysis. IPS analyses require no input from solar surface flare determinations or modeling from coronagraph inputs to provide short-term predictions of heliospheric transient events such as CMEs. At the KSWC, both the IPS kinematic 3-D reconstructions and the ENLIL model are running side by side in a prediction scheme to help forecast geomagnetic storms at Earth. Typically, ENLIL modeling plus inputs from coronagraphs to map CMEs and determine their additional input to a background heliosphere, takes considerable manpower and expertise to implement. In these analyses, fits of CMEs are generally best provided manually using all available coronagraph inputs within hours of their observation. This requires 24 h attendance from well-instructed forecasters as well as the availability of real-time coronagraph data. In a hybrid prediction system using IPS, no intervention is needed other than an occasional check to determine that all the inputs and programs are operating correctly and thus requires little manpower to provide a prediction for forecast purposes. Many of the input parameters to the 3-D MHD modeling are poorly known, and some crucial model settings are best guesses of the correct values, and these inputs can affect the model results differently for different events. Gamma (the ratio of specific heat capacity), for instance, is generally assumed the same at all distances from the Sun in the inner heliosphere. *Wu et al.* [2011] find its value to be near 5/3. This value is usually assumed to be the same for solar wind constituents other than protons and applied equally to them in all events. Similarly, for the MHD modeling, temperature is constrained only within wide limits. With correct values of velocity and density definitively specified by direct measurements at 1 AU, and approximated at the lower boundary by the IPS analysis, both gamma and temperature can be studied and modified to provide consistent results by comparing the two techniques. If they can be shown to consistently provide better predictions, the 3-D MHD modeling and 3-D reconstruction analyses are both expected to improve. This improvement can be shown in archival scientific determinations of solar wind structure morphology and their interactions, the validation and improvement of the modeling techniques, and better ways to analyze different IPS data sets.

2. Near Real-Time IPS Boundary Values for the ENLIL 3-D MHD Model

Our tomographic inversion analysis uses a source surface below all IPS lines of sight and propagates the iterative kinematic model upward from this surface. These lines of sight are required to have greater than 11.5° elongation with IPS observations obtained in the region of weak scattering [*Tatarski*, 1961] at 327 MHz. The STELab tomographic analysis has a 24 h cadence, at a latitude and longitude resolution of 20° in heliographic coordinates. Volumetric results from this analysis are presented in heliographic coordinates and smoothed to a 6 h cadence, generally starting at 15.0 R_s (~0.07 AU) and progressing outward in steps of 0.025 AU, to a final distance of 3.0 AU from the solar surface.

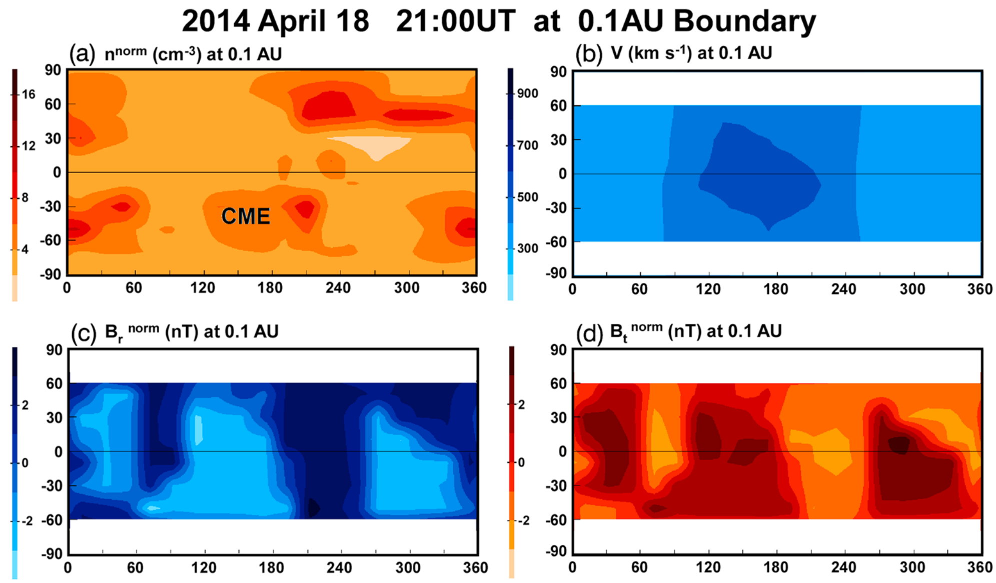

Figure 3. HEEQ coordinate boundary maps at 21.5 R_s at 21:00 UT 18 April 2014 used by ENLIL. At this time, the Earth is ~5° south of the heliographic equator. (a) Density: these are normalized to 1 AU by an r^{-2} falloff. The dense region to the south of the heliographic equator is associated with a halo CME observed in the LASCO coronagraphs (see section 3). (b) Velocity. (c) Radial magnetic field: this is normalized to values at 1 AU by an r^{-2} falloff. (d) Tangential magnetic field: this is normalized to values at 1 AU by an r^{-1} falloff.

In forming a boundary for ENLIL, the heliographic coordinate system specific to the IPS 3-D reconstruction (version 14) is interpolated at a solar distance of 21.5 R_s and transformed into the inertial Heliocentric Earth Equatorial (HEEQ) system used by ENLIL; additionally, the IPS global values are interpolated into the 4° low-resolution numerical grid used by ENLIL (version 2.8 modified for UCSD IPS boundary inputs). The 3-D reconstruction is updated every 6 h and is available for download on a UCSD ftp server. These files include values of density, velocity, and radial and tangential magnetic fields for 20 days prior to and 4 days following the time of the 3-D reconstruction run. Figure 3 shows the images from a typical set of files. Here in April 2014, no IPS velocities are available from STELab, and thus, velocities are presented along the solar equator as projected at 3-D reconstruction resolutions from Earth-based measurements assuming that the Sun corotates [see *Jackson et al.*, 2012, 2013]. We do not present velocities or magnetic fields beyond 60° because they are simply extrapolations from lower latitude values. When velocities are available from IPS observations, these boundaries are filled to show global transient velocities. Magnetic fields are generally not available over the poles regardless and are interpolated from lower latitude values where the field measurements are available. These are then extrapolated globally from velocity measurements to provide magnetic fields of higher reliability than a simple extrapolation from near latitudinal values at any given solar distance [see *Yu et al.*, 2012]. Production of these is usually completed in approximately 10 min following the completion of the 3-D reconstruction program. The boundaries are placed on an ftp website for download to other sites with a cadence of 6 h. Once these boundaries are transferred to a workstation that runs ENLIL, they provide input to the 3-D MHD program using appropriate scaling factors.

3. ENLIL Operation Using IPS Boundary Values

The ENLIL 3-D MHD computations on a low-resolution grid generally take about 12 min to complete. Generating the prediction images generally adds another 30 min. Figure 4 shows one of several prediction outputs as produced from an ENLIL run on an experimental test site at the George Mason University (GMU), Space Weather Laboratory, Maryland, USA, which hosts a test analysis at http://spaceweather.gmu.edu/projects/enlil/models/ipsbd/den1r2e4b/index.html and also at http://helioweather.net/. For this case, STELab IPS data were available up until 07:00 UT on 19 April 2014. Processing at STELab currently takes another 10 h after which the data are downloaded and boundary values are produced and placed on the UCSD ftp

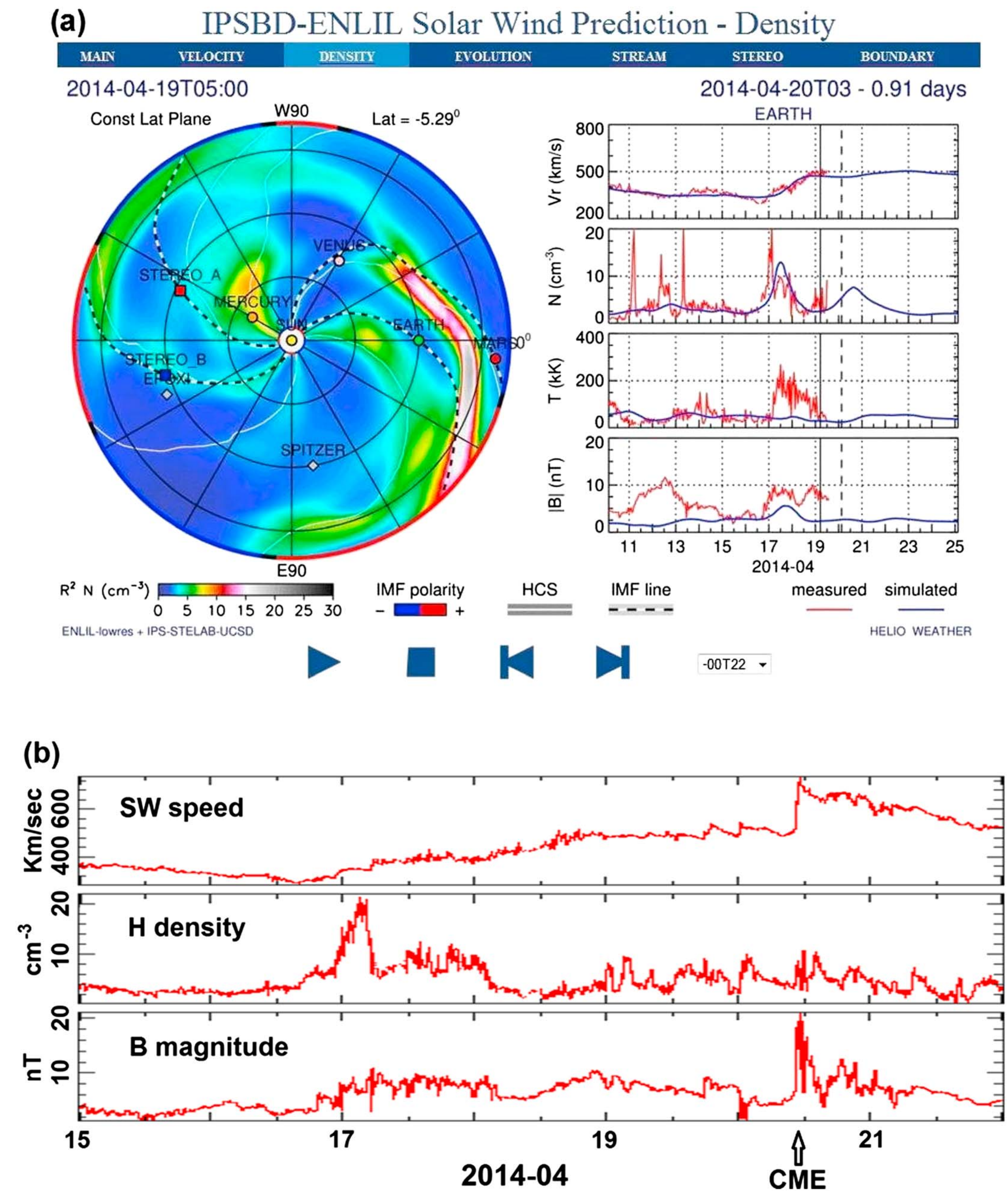

Figure 4. (a) ENLIL results at 05:00 UT on 19 April 2014 (solid vertical line in Figure 4a, right) from a near real-time GMU analysis of STELab IPS data provided at 03:00 UT on 20 April 2014 (dashed vertical line in Figure 4a, right). Density, normalized to 1 AU by an r^{-2} falloff (Figure 4a, left). Measured and ENLIL-simulated values of density, velocity, temperature, and magnetic field magnitude (Figure 4a, right). (b) Density, velocity, and magnetic field magnitude in situ values from ACE throughout the period of CME arrival on ~11:30 UT 20 April as marked on the time series.

website. Figures 4a and 5, a successful sample prediction (see below), were shown at the Korean Space Science Society meeting on 25 April held in Buyeo, South Korea [*Jackson et al.*, 2014].

The sample ENLIL prediction shows a halo CME, in both the latitudinal cut and the in situ ACE beacon density data, that is expected to arrive midday on 20 April 2014. An alert about this CME was presented by *Schenk* [2014] in a report at 19:30 UT on 18 April. In this Large Angle Spectrographic Coronagraph (LASCO) [*Brueckner et al.*, 1995] analysis, "SOHO/LASCO observed two halo CMEs in close succession 18 April 2014. The events are first seen in C2 at 13:25 UT as a bright loop in progress over the southwest. The front expands with extensions to a full halo CME by 13:36 UT. The event continues into the C3 field beginning 13:30 to 17:42 UT leaving the

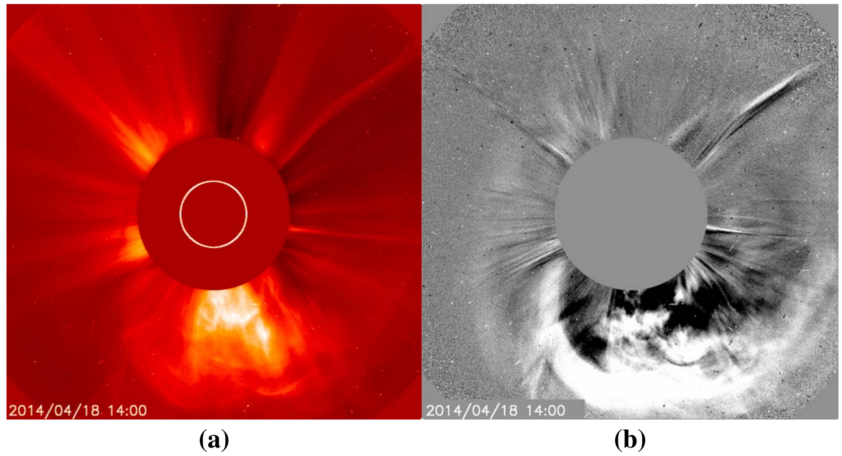

Figure 5. (a) LASCO C2 image of the halo CME sequence of 18 April 2014 obtained at 14:00 UT. (b) A LASCO C2 difference image obtained by subtracting a LASCO image obtained just prior to the one at 14:00 UT in order to show more CME detail than can be viewed in the single image of Figure 5a which has its long-term base removed.

C3 field of view at 30 R_s in the south." At the Sun, the event appeared as a large CME (Figure 5), and it was associated with a solar energetic proton (SEP) event observed at Earth (see http://umbra.nascom.nasa.gov/SEP/) beginning at 15:25 UT on 18 April 2014.

At the time of the CME, there was concern at the KSWC that this event would cause a large geomagnetic effect in addition to the observed SEP response at Earth. When the IPS-ENLIL prediction (Figure 4a) was available, the CME had not yet arrived at Earth, and this analysis showed that the event was propagating rather slowly along the Sun-Earth line and expected to arrive at Earth almost 3 days following its initiation with a minimal enhancement in density. Indeed, evidence that the halo CME manifestation arrived at 1 AU is present in the L_1 browse record from ACE at about the time predicted for the maximum response time in the IPS-driven ENLIL modeling, as shown in Figure 4b. At this time, there is a magnetic field enhancement followed by a velocity enhancement but very little evidence of increased density in the ACE data. A more complete analysis of this event that includes an out-of-the-ecliptic determination of its density, as in Figure 3a, shows that the bulk of this CME brushed past Earth to the south and that the Earth was never directly in line with the major portion of the CME response. Although this is a halo CME, this southerly direction of CME material is also indicated in the coronagraph observations (see Figure 5) nearer the Sun than shown in the IPS analyses. The kinematic IPS analysis at UCSD and at the KSWC (see Figure 2) for this interval also predicted the correct response. In situ ACE observations and those from CELIAS give rather different (if small) density enhancements of this event's passage. There was little substorm activity caused by the event since the magnetic field did not go southward for a sustained period when the event arrived.

We note that predicted temperatures and magnetic fields are not presently well matched by in situ measurements at ACE shown in Figure 4a; improving this for ENLIL forward-modeling analyses is a major future objective for this ongoing research.

Analyses with the IPS-driven ENLIL system are more immediately expected to refine IPS-driven ENLIL boundary parameter scaling and provide a better 3-D MHD-free parameter determination to use with this technique. This type of parameter establishment and validation can proceed in a way similar to that shown for the 2 month comparison sequence in Figures 6 and 7. Here the time series from the IPS kinematic analysis and the IPS-driven hydrodynamic ENLIL model are compared as in H.-S. Yu et al. (3D Reconstruction of Interplanetary Scintillation (IPS) Remote-Sensing Data: Global Solar Wind Boundaries for Driving 3D-MHD Models, submitted to *Solar Physics*, 2014] incorporating Wind spacecraft in situ measurements. The comparison validity is established by a Pearson's "*R*" correlation that shows how well the modeled analysis agrees with in situ measurements. In this type of analysis, a perfect correlation of data provides a straight line of data points. Further, a one-to-one correlation shows agreement in magnitude. In a forecast analysis, two types of correlations are possible and have been experimented with at UCSD using the

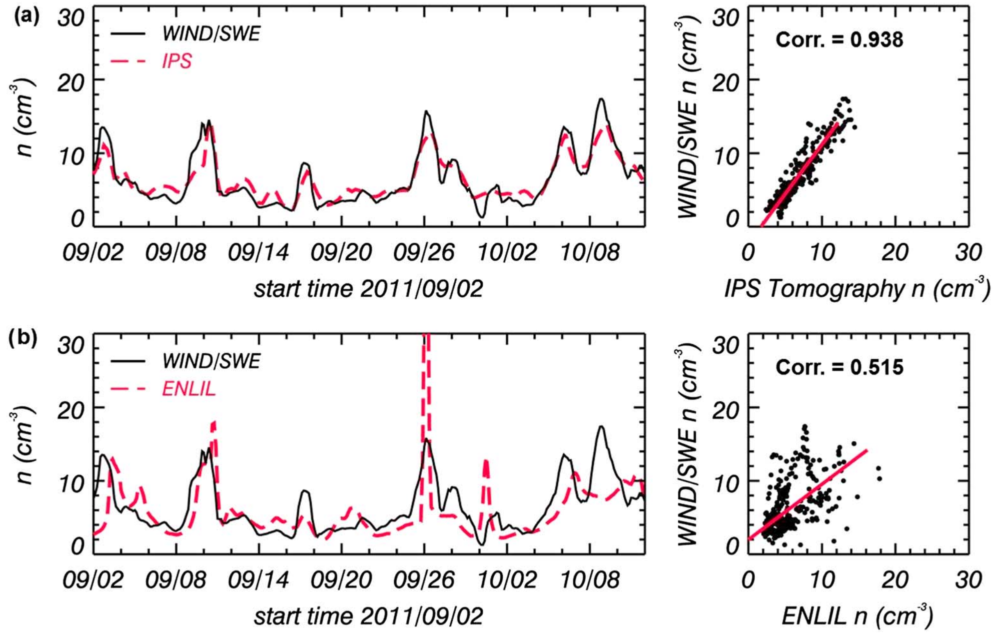

Figure 6. (a) Comparison of the UCSD IPS kinematic density analysis results with the Wind in situ density data for the period from 2 September to 12 October 2011. The Wind density measurements have been averaged with a 1 day boxcar to match the resolution of the IPS analysis. Time series superimposed (Figure 6a, left). Pearson's *R* correlation of the two time series (Figure 6a, right). (b) Same as in Figure 6a but for the IPS-driven ENLIL density model analysis.

kinematic IPS 3-D reconstructions. The first, shown online at http://ips.ucsd.edu, provides a correlation between the IPS-derived predictions 1 day into the future from the time the analysis is run and then compared with the actual value 1 day later. Comparison between the predicted value and the measured value provides the correlation. A one-to-one response shows that the forecast values are correctly

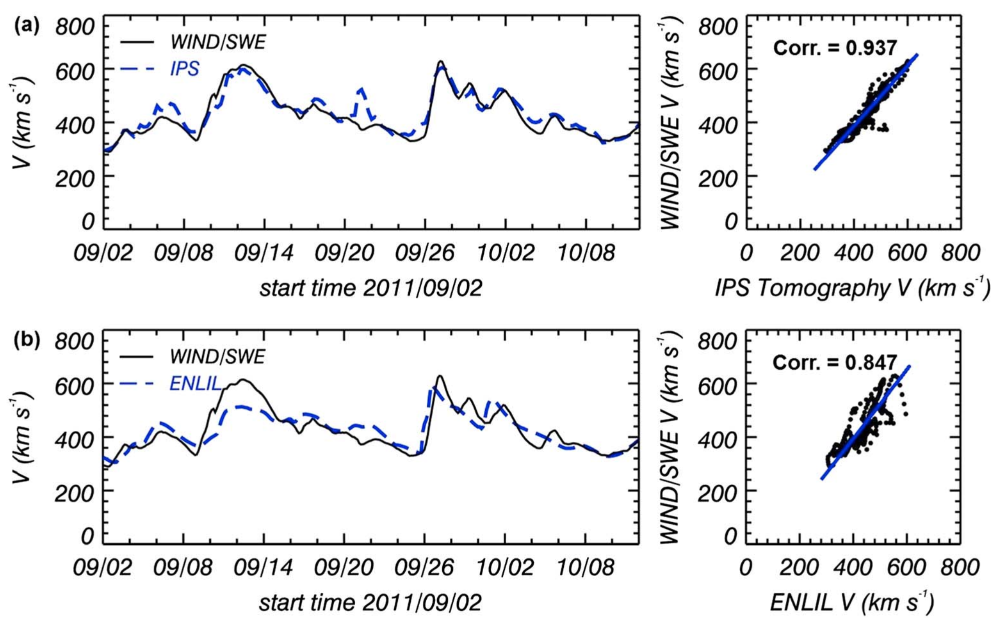

Figure 7. (a) Comparison of the UCSD IPS kinematic velocity analysis results with the Wind in situ velocity data for the period from 2 September to 12 October 2011. The Wind velocity measurements have been averaged with a 1 day boxcar to match the resolution of the IPS analysis. Time series superimposed (Figure 7a, left). Pearson's *R* correlation of the two time series (Figure 7a, right). (b) Same as in Figure 7a but for the IPS-driven ENLIL velocity model analysis.

determined in magnitude. A second way to do this is described in *Jackson et al.* [2013]. Here the differences from the measured value at the run time from the measured values 1, 2, and 3 ahead of the run time at Earth are compared with similarly predicted difference values. We have found that both correlation techniques operated for monthlong stretches of data analyses give similar results 1 day ahead of the run time. For the analysis of 1 month stretches of data for a 7 month period in 2011, *Jackson et al.* [2013] found correlations of the change considerably better than by assuming persistence (the value remaining the same as at the run time) 1 and 2 days ahead. At 3 days ahead of the run time, the analysis breaks down since this prediction time, which includes the latency from when the sources were observed before the run time, is on average slightly greater than the limit from when heliospheric structures are first observed by the IPS system until they reach Earth along the Sun-Earth radial. We also find that the correlations 1 day ahead break down, during specific portions of the year, and especially in the late summer in Japan when typhoons generally cross the country causing many array outages. Following a single analysis that can be used to refine parameters in the IPS-driven ENLIL program, as in Figures 6 and 7, to find the best *R* and one-to-one correlation using contemporary data sets, we can then operate a system as has been done in the past using the IPS kinematic model to provide similar refinements for the predictive analyses. The operational analysis at the KSWC has been established to provide real-time predictions using this IPS-driven ENLIL system and these validations. This type of comparison takes many runs of the analysis over extended time intervals following each model parameter change and is beyond the scope of the current article.

The analyses shown in Figures 6 and 7 display clear differences. Neither the kinematic analysis nor IPS-driven ENLIL is perfectly correlated with the near-Earth Wind in situ measurements. The kinematic model, however, fits better for both density and speed. This is likely due to the fact that the kinematic model iterates to find a best fit to the observational data, while ENLIL is a forward-model that derives heliospheric values from an inner boundary. ENLIL velocities fit the Wind in situ measurements well (or those from ACE—not shown) better than for the in situ density values. Velocities are the key to how rapidly outward solar wind features propagate from the Sun to arrive at Earth and the inner planets. Traditionally, the most attention has been given to matching solar wind velocities since this is of prime importance for the propagation of transient disturbances. There has been less emphasis on how well ENLIL fits density results, since densities are not measured as well in previous 3-D MHD forecasting using proxy information near the Sun. Additionally, the arrival time of fast-mode shocks propagated by CMEs has more to do with the ambient medium and the CME speed than the CME density. One notable CME event shown arriving midday on 26 September 2012 in Figures 6 and 7 is seen from the in situ data to be two shocks associated with at least one extremely energetic 2000 km s^{-1} CME observed by LASCO C2 that began at the Sun midday on 24 September. Although this CME decreased in speed significantly as it moved outward toward the inner boundary used by ENLIL, its speed is nevertheless well represented in the IPS boundary observations (H.-S. Yu et al., submitted manuscript, 2014). The main shock from this CME appears far more enhanced in the IPS-driven model than in the actual in situ measurements at 1 AU. Some recent work with ENLIL suggests how to reduce these peaks so that they do not present such a large enhancement (D. Odstrcil et al., Numerical prediction of heliospheric space weather using interplanetary scintillation data boundary conditions: The IPSBD-ENLIL modeling system, in preparation for *Space Weather*, 2015). More careful modeling of shock densities should immediately provide more realistic J-map matches of ENLIL Thomson-scattering simulations to coronal and heliospheric imaging observations as in *Lugaz et al.* [2011] and *Odstrcil* [2012] for use with existing ENLIL modeling techniques.

4. Summary and Conclusions

The resolution of UCSD IPS 3-D reconstruction predictions depends very strongly on the numbers of radio sources that can be observed in the sky near the Sun over the period preceding the heliospheric structure arrival at any given location in space. The STELab array systems, designed primarily for heliospheric research, are limited in the numbers of radio sources they can observe. This limit is caused primarily by the collecting area of the array system, and the number of point-like radio sources at a given radio frequency that can be used to provide a scintillating flux. For the largest (3432 m^2) STELab IPS radio antenna (Solar Wind Imaging Facility (SWIFT)) [*Tokumaru et al.*, 2011] that began full operation near Toyokawa, Japan, in late 2010, the number of sources that can be observed with a transit instrument such as this is limited to about 200. Providing a forecast resolution with better than about a 1 day cadence and a 15°×15° latitude and longitude spatial resolution is about the limit for this system. Other systems around the world have larger collecting areas and can observe considerably greater numbers of radio sources. These include the 15,900 m^2 Ooty system in India and the 70,000 m^2 BSA in Russia. Each, reportedly capable of measuring greater than 10,000 scintillating sources per day, would in theory allow about the cube root of the observed source number difference in resolution of the current STELab system, or temporal resolutions of about 6 h, and spatial resolutions of about 4° × 4° in latitude and longitude. Unfortunately, neither the Ooty nor the BSA groups have so far had the resources to provide their observational data in near real time for use in these predictive analyses.

Space weather forecast centers are concerned with many aspects of heliospheric constituents at Earth and globally: corotating heliospheric features, CMEs, high-energy particle fluxes, etc. For CME propagation, there is generally more emphasis on a determination of the CME onset at any specific heliospheric location rather than a prediction of the speed and density change associated with its propagation. This is because the most crucial factor contributing to a geoeffective response at Earth is a CME's associated vector magnetic field, and currently, this is poorly known for any specific event. In an operational setting, it makes good sense to provide a single criterion for success (i.e., the arrival time of CMEs), but to improve the modeling of a prediction process, it is often important to explore additional adjustments, both to data inputs and the modeling itself. Large imaging ground-based radio arrays are currently designed to measure polarized signals from naturally occurring radio sources at large elongations from the Sun. These signals have the possibility to measure Faraday rotation from these sources [*Oberoi and Lonsdale*, 2012], and observations of heliospheric signals have already been claimed from the Low-Frequency Array in Netherlands [*Bisi et al.*, 2014] and are an actively pursued topic with the Murchison Widefield Array in Western Australia. Faraday rotation is a linear integral combination of density and the field vector parallel to the LOS. If Faraday rotation observations become commonplace, then determining the magnitude of the field will require detailed 3-D density measurements that result from the accurate heliospheric modeling and not simply the onset timing of heliospheric structures. Refining the timing metric for onset at Earth would be important but probably not as great as determining vector fields including the ability to back out measurement of the magnitude of a sustained negative B_z using this technique. Such a procedure once implemented should significantly advance this aspect of heliospheric space weather forecasting.

Although the analysis presented here refines the parameters needed in the 3-D MHD modeling, an even more significant gain should result if the 3-D MHD modeling is used as a kernel to provide an iterative time-dependent solution that fits the IPS data, i.e., to incorporate it into the 3-D reconstruction process. Only then will the better physics provided by 3-D MHD modeling be optimized for a prediction model capable of significantly improved heliospheric updates.

When and if the additional IPS systems mentioned above in section 1.1 contribute to the global IPS data sets, the network of longitudinally separated systems will become more robust for use in forecasting since the prediction analysis will no longer depend on a single site for input. This is important when outages at one system occur so that they can be covered by the other system. One of the biggest drawbacks of a single-system IPS operation is that one array can only view radio sources near the Sun while it transits; nighttime on Earth is a period where very fast CMEs can escape detection on their way to Earth. The very fast CMEs can arrive at Earth before an array at any given longitude can observe it coming outward along the Sun-Earth line. Thus, inputs from different longitudes or even two sites stationed on opposite sides of the globe will enable better coverage such that even the fastest CME cannot pass undetected throughout a 24 h period. Better longitude coverage will also yield a better prediction of CME Earth arrival from the additional data available, or in case, one or the other of the systems has an outage. Additionally, any latency present from one site where data cannot be immediately processed will not be as large an issue for the remotely sensed IPS analysis when many sites are contributing data. In these instances, the first site to yield data provides a preview, and additional data provide updates as they become available.

Acknowledgments
The KSWC initiated and have supported this project from its onset with partial funding to B.V. Jackson and D. Odstrcil. In addition, B.V. Jackson, H.-S. Yu., and A. Buffington have been partially funded by AFOSR contract FA9550-11-1-0324 and NSF contracts AGS-1053766 and AGS-1358399 to the University of California, San Diego. J. Mejia-Ambriz thanks and acknowledges his support from the UC MEXUS CONACyT program while at UCSD. D. Odstrcil also acknowledges support from the NASA/NSF LWS Partnership for Collaborative Space Weather Modeling program Collaborative Space Weather 11-LWSCSW11-0034 project for this effort. The SWIFT IPS observations were carried out under the solar wind program of the Solar-Terrestrial Environment Laboratory (STELab) of Nagoya University. The STELab near-real-time IPS observations used in these analyses are available online at ftp://ftp.stelab.nagoya-u.ac.jp/pub/vlist/rt/. We are grateful for the SOHO LASCO team and especially K. Schenk for providing alerts (e-mail: Soho-halo-alert@grace.nascom.nasa.gov) and for making available the LASCO C2 and C3 observations at http://umbra.nascom.nasa.gov/lasco/observations/halo/2014/140418ab/ used in these analyses. We thank the ACE spacecraft group for making their data available in real time for use at UCSD through the Space Weather Prediction Center, NOAA, Boulder, and for Figure 4 at http://www.swpc.noaa.gov/ftpdir/lists/ace2/ and to the Wind spacecraft group for making their data available for Figures 6 and 7 at ftp://space.mit.edu/pub/plasma/wind/kp_files_hr_aves/. A special thanks is warranted for the SOHO/CELIAS data made available to UCSD in near real time by the Proton Monitor group at the University of Maryland, College Park, USA at ftp://space.umd.edu/pm/houraverages.txt.

References

Ananthakrishnan, S., W. A. Coles, and J. J. Kaufman (1980), Microturbulence in solar wind streams, *J. Geophys. Res.*, *85*, 6025–6030, doi:10.1029/JA085iA11p06025.

Arge, C. N., and V. J. Pizzo (2000), Improvement in the prediction of solar wind conditions using near-real time solar magnetic field updates, *J. Geophys. Res.*, *105*, 10,465–10,479, doi:10.1029/1999JA000262.

Behannon, K. W., L. F. Burlaga, and A. Hewish (1991), Structure and evolution of compound streams at ≤1 AU, *J. Geophys. Res.*, *96*, 21,213–21,225, doi:10.1029/91JA02267.

Bisi, M. M., B. V. Jackson, P. P. Hick, A. Buffington, and J. M. Clover (2007), Coronal mass ejection reconstructions from interplanetary scintillation data using a kinematic model: A brief review, *Adv. Geosci.*, *14*, 161–181.

Bisi, M. M., B. V. Jackson, A. Buffington, P. P. Hick, P. K. Manoharan, and J. M. Clover (2008), Solar wind and CME reconstructions in the inner heliosphere, *Adv. Geosci.*, *21*, 1–17.

Bisi, M. M., B. V. Jackson, J. M. Clover, P. K. Manoharan, M. Tokumaru, P. P. Hick, and A. Buffington (2009), 3D reconstructions of the early-November 2004 CDAW geomagnetic storms: Analysis of Ooty IPS speed and density data, *Ann. Geophys.*, *27*, 4479–4489.

Bisi, M. M., R. A. Fallows, E. A. Jensen, B. V. Jackson, C. Sobey, I. Cairns, and D. Oberoi (2014), Progress on the use of Low Frequency Radio Telescopes for space weather related activities, ST23-A015 oral presentation at the annual AOGS meeting, Sapporo, Japan, 28 July–1 Aug. [Available at http://www.asiaoceania.org/society/public.asp?bg=abstract&page=absList14/listBySection.asp#sID_65.]

Brueckner, G. E., et al. (1995), The Large Angle Spectroscopic Coronagraph (LASCO), *Solar Phys.*, *162*, 357–402.

Chashei, I., V. Shishov, S. Tyul'bashev, I. Subaev, and V. Oreshko (2013), Results of IPS observations in the period near solar activity minimum, *Solar Phys.*, *285*, 141–149.

Domingo, V., B. Fleck, and A. I. Poland (1995), SOHO: The Solar and Heliospheric Observatory, *Space Sci. Rev.*, *72*, 81–84.

Dunn, T., B. V. Jackson, P. P. Hick, A. Buffington, and X. P. Zhao (2005), Comparative analyses of the CSSS calculation in the UCSD tomographic solar observations, *Solar Phys.*, *227*, 339–353.

Gapper, G. R., A. Hewish, A. Purvis, and P. J. Duffet-Smith (1982), Observing interplanetary disturbances from the ground, *Nature*, *296*, 633–636.

Hayashi K., M. Kojima, M. Tokumaru, and K. Fujiki (2003), MHD tomography using interplanetary scintillation measurements, *J. Geophys. Res.*, *108*(A3), 1102, doi:10.1029/2002JA009567.

Hayashi, M. (2012), An MHD simulation model of time-dependent co-rotating solar wind, *J. Geophys. Res.*, *117*, A08105, doi:10.1029/2011JA017490.

Hewish, A., and S. Bravo (1986), The sources of large-scale heliospheric disturbances, *Solar Phys.*, *106*, 185–200.

Hewish, A., P. F. Scott, and D. Wills (1964), Interplanetary scintillation of small diameter radio sources, *Nature*, *203*, 1214–1217.

Hick, P. P., and B. V. Jackson (2004), Heliospheric tomography: An algorithm for the reconstruction of the 3D solar wind from remote sensing observations, in *Proc. SPIE*, *5171*, edited by S. Fineschi and M. A. Gummin, pp. 287–297.

Houminer, Z. (1971), Correlation of interplanetary scintillation and spacecraft plasma density measurements, *Nature Phys. Sci.*, *231*, 165–167.

Hovestadt, D., et al. (1995), CELIAS—Charge, Element and Isotope Analysis System for SOHO, *Solar Phys.*, *162*, 441–481, doi:10.1007/BF00733436.

Jackson, B. V., and P. P. Hick (2005), Three-dimensional tomography of interplanetary disturbances, in *Solar and Space Weather Radiophysics, Current Status and Future Developments*, *Astrophys. Space Sci. Lib.*, vol. 314, edited by D. E. Gary and C. U. Keller, chap. 17, pp. 355–386, Kluwer Acad., Dordrecht, Netherlands.

Jackson, B. V., P. L. Hick, M. Kojima, and A. Yokobe (1998), Heliospheric tomography using interplanetary scintillation observations: 1. Combined Nagoya and Cambridge data, *J. Geophys. Res.*, *103*, 12,049–12,068, doi:10.1029/97JA02528.

Jackson, B. V., P. P. Hick, A. Buffington, M. Kojima, M. Tokumaru, K. Fujiki, T. Ohmi, and M. Yamashita (2003), Time-dependent tomography of hemispheric features using interplanetary scintillation (IPS) remote-sensing observations, in *Solar Wind Ten*, *Am. Inst. Phys. Conf. Ser.*, vol. 679, edited by M. Velli, R. Bruno, and F. Malara, pp. 75–78.

Jackson, B. V., J. A. Boyer, P. P. Hick, A. Buffington, M. M. Bisi, and D. H. Crider (2007), Analysis of solar wind events using interplanetary scintillation (IPS) remote sensing 3D reconstructions and their comparison at Mars, *Solar Phys.*, *241*, 385–396.

Jackson, B. V., P. P. Hick, A. Buffington, M. M. Bisi, J. M. Clover, and M. Tokumaru (2008), Solar Mass Ejection Imager (SMEI) and interplanetary scintillation (IPS) 3D-reconstructions of the inner heliosphere, *Adv. Geosci.*, *21*, 339–366.

Jackson, B. V., P. P. Hick, M. M. Bisi, J. M. Clover, and A. Buffington (2010a), Inclusion of in-situ velocity measurements in the UCSD time-dependent tomography to constrain and better-forecast remote-sensing observations, *Solar Phys.*, *265*, 245–256, doi:10.1007/s11207-010-9529-0.

Jackson, B. V., A. Buffington, P. P. Hick, J. M. Clover, M. M. Bisi, and D. F. Webb (2010b), SMEI 3-D reconstruction of an ICME interacting with a co-rotating solar wind density enhancement: The 26 April 2008 CME, *Astrophys. J.*, *724*, 829–834.

Jackson, B. V., P. P. Hick, A. Buffington, M. M. Bisi, J. M. Clover, M. Tokumaru, M. Kojima, and K. Fujiki (2011), Three-dimensional reconstruction of heliospheric structure using iterative tomography: A review, *J. Atmos. Sol. Terr. Phys.*, *73*, 1214–1227.

Jackson, B. V., P. P. Hick, A. Buffington, J. M. Clover, and M. Tokumaru (2012), Forecasting transient heliospheric solar wind parameters at the locations of the inner planets, *Adv. Geosci.*, *30*, 93–115.

Jackson, B. V., J. M. Clover, P. P. Hick, A. Buffington, M. M. Bisi, and M. Tokumaru (2013), Inclusion of real-time in-situ measurements into the UCSD time-dependent tomography and its use as a forecast algorithm, *Solar Phys.*, *285*, 151–165.

Jackson, B. V., H.-S. Yu, P. Hick, A. Buffington, D. Odstrcil, S. Hong, J. Kim, and M. Tokumaru (2014), 3D analysis of remote-sensed heliospheric data for space weather forecasting, oral presentation at the Korean Space Science Society meeting, Buyeo, South Korea, 23–25 April. [Available at ftp://cass185.ucsd.edu/Presentations/2014_Buyeo.]

Kim, J.-H., and J. No (2013), Site report Korean IPS system at KSWC, Presentation at the 2013 STELab IPS Workshop, Nagoya, 23–24 Nov.

Kim, T. K., S. N. Borovikov, N. V. Pogorelov, H.-S. Yu, J. M. Clover, and B. V. Jackson (2012), Time-dependent MHD simulations of the solar wind outflow using interplanetary scintillation observations, in *AIP Conference Proceedings, 1500, Space Weather: The Space Radiation Environment, 11th Annual International Astrophysics Conference (CSPAR)*, edited by Q. Hu et al., pp. 140–146, Palm Springs, Calif.

Kim, T. K., N. V. Pogorelov, S. N. Borovikov, B. V. Jackson, H.-S. Yu, and M. Tokumaru (2014), MHD heliosphere with boundary conditions from a tomographic reconstruction using interplanetary scintillation data, *J. Geophys. Res. Space Physics*, *119*, 7981–7997, doi:10.1002/2013JA019755.

Kojima, M., and T. Kakinuma (1987), Solar cycle evolution of solar wind speed structure between 1973 and 1985 observed with the interplanetary scintillation method, *J. Geophys. Res.*, *92*, 7269–7279, doi:10.1029/JA092iA07p07269.

Kojima, M., M. Tokumaru, H. Watanabe, A. Yokobe, K. Asai, B. V. Jackson, and P. L. Hick (1998), Heliospheric tomography using interplanetary scintillation observations: 2. Latitude and heliocentric distance dependence of solar wind structure at 0.1–1 AU, *J. Geophys. Res.*, *103*, 1981–1989, doi:10.1029/97JA02162.

Kojima, M., M. Tokumaru, K. Fujiki, Y. Ishida, T. Ohmi, K. Hayashi, and M. Yamashita (2002), Solar wind imaging facility for space weather research, *Proc. SPIE, Waikoloa, 4853*, 121–128, doi:10.1117/12.460271.

Lugaz, N., I. I. Roussev, and T. I. Gombosi (2011), Determining CME parameters by fitting heliospheric observations: Numerical investigation of the accuracy of the methods, *Adv. Space Res.*, *48*, 292–299.

MacNeice, P. J. (2012), SHINE Working Group Session: Community-wide validation study of models of the corona and inner heliosphere', SHINE 12 Workshop, Maui, Hawaii, 25–29 June. [Available at http://shinecon.org/shine2012/ViewUsBySessions12.php.]

MacNeice, P. J., A. Taktakishvili, B. V. Jackson, J. M. Clover, M. M. Bisi, and D. Odstrcil (2011), Comparative validation of realtime solar wind forecasting using the UCSD heliospheric tomography model, paper presented at AGU Fall Meeting Program, SH31C-2026, San Francisco, Calif., 5–9 Dec.

Manoharan, P. K. (2010), Ooty interplanetary scintillation–remote-sensing observations and analysis of coronal mass ejections in the heliosphere, *Solar Phys.*, *265*, 137–157.

McComas, D. J., S. J. Bame, P. Barker, W. C. Feldman, J. L. Phillips, P. Riley, and J. W. Griffee (1998), Solar Wind Electron Proton Alpha Monitor (SWEPAM) for the Advanced Composition Explorer, *Space Science Revs.*, *86*, 563–612.

Mejia-Ambriz, J. C., P. Villanueva-Hernandez, J. A. Gonzalez-Esparza, S. Aguilar-Rodriguez, and S. Jeyakumar (2010), Observations of interplanetary scintillation (IPS) using the Mexican Array Telescope (MEXART), *Solar Phys.*, *265*, 309–320.

Meng, X. (2013), Connecting remote-sensing observations and MHD modeling towards a new generation of space weather prediction tools, proposal to the UCAR NASA LWS Program.

Oberoi, D., and C. J. Lonsdale (2012), Media responsible for Faraday rotation: A review, *Radio Sci.*, *47*, RS0K08, doi:10.1029/2012RS004992.

Odstrcil, D. (2003), Modeling 3-D solar wind structure, *Adv. Space Res.*, *32*, 497–506, doi:10.1016/S0273-117(03)00332-6.

Odstrcil, D. (2012), ENLIL: Modeling of heliospheric space weather, CCMC Workshop, Key Largo, Fla., 16–20 Jan. [Available at http://ccmc.gsfc.nasa.gov/RoR_WWW/workshops/2012/Monday_pdf/odstrcil_ccmc2012.pdf.]

Odstrcil, D., and V. J. Pizzo (1999), Three-dimensional propagation of coronal mass ejections (CMEs) in a structured solar wind flow: 1. CME launched within the streamer belt, *J. Geophys. Res.*, *104*(A1), 483–492, doi:10.1029/1998JA900019.

Odstrcil, D., V. J. Pizzo, C. N. Arge, B. V. Jackson, and P. P. Hick (2005), First results from the 3-D MHD heliospheric simulations driven by the SMEI/IPS observations, presented at SPIE 50th Annual Meeting on Optics & Photonics, San Diego, Calif., July.

Odstrcil, D., et al. (2007), ENLIL at the CCMC, CCMC Workshop, Arecibo, Puerto Rico, 5–8 Nov. [Available at http://ccmc.gsfc.nasa.gov/RoR_WWW/workshops/2007/presentations/day2/Odstrcil.pdf.]

Odstrcil, D., et al. (2008), Numerical simulations of solar wind disturbances by coupled models, ASP Conference Series Proceedings, 385, 167–173.

Schenk, K. (2014), 18 April Soho-halo-alert, 140418ab. [Available at http://umbra.nascom.nasa.gov/lasco/observations/halo/2014/140418ab/.]

Scherrer, P. H., et al. (2012), The Helioseismic and Magnetic Imager (HMI) investigation for the Solar Dynamics Observatory (SDO), *Sol. Phys.*, *275*, 207–227.

Shibata, K., and Y. Kamide (2007), Basic study of space weather predictions: A new project in Japan, *Space Weather*, *5*, S12006, doi:10.1029/2006SW000306.

Stone, E. C., A. M. Frandsen, R. A. Mewaldt, E. R. Christian, D. Margolies, J. F. Ormes, and F. Snow (1998), The Advanced Composition Explorer, *Space Sci. Rev.*, *86*, 1–22.

Tatarski, V. I. (1961), *Wave Propagation in a Turbulent Medium*, McGraw-Hill, New York.

Tokumaru, M. (2013), Three-dimensional exploration of the solar wind using observations of interplanetary scintillation, *Proc. Jpn. Acad. B*, *89*, 67.

Tokumaru, M., M. Kojima, K. Fujiki, K. Maruyama, Y. Maruyama, H. Ito, and T. Iju (2011), A newly developed UHF radiotelescope for interplanetary scintillation observations: Solar Wind Imaging Facility, *Radio Sci.*, *46*, RS0F02, doi:10.1029/2011RS004694.

Toth, G., et al. (2012), Adaptive numerical algorithms in space weather modeling, *J. Comput. Phys.*, *231*, doi:10.1016/j.jcp.2011.02.006.

Wu, C.-C., C. D. Fry, S. T. Wu, M. Dryer, and K. Liou (2007), Three-dimensional global simulation of interplanetary coronal mass ejection propagation from the Sun to the heliosphere: Solar event of 12 May 1997, *J. Geophys. Res.*, *112*, A09104, doi:10.1029/2006JA012211.

Wu, C.-C., M. Dryer, S. T. Wu, B. E. Wood, C. D. Fry, K. Liou, and S. Plunkett (2011), Global three-dimensional simulation of the interplanetary evolution of the observed geoeffective coronal mass ejection during the epoch 1–4 August 2010, *J. Geophys. Res.*, *116*, A12103, doi:10.1029/2011JA016947.

Yu, H.-S., B. V. Jackson, P. P. Hick, A. Buffington, J. M. Clover, and M. Tokumaru (2012), 3-D reconstruction of the inner heliosphere from remote-sensing data: A global solar wind boundary that includes CME transient effects, in *AIP Conference Proceedings, 1500, Space Weather: The Space Radiation Environment, 11th Annual International Astrophysics Conference (CSPAR)*, edited by Q. Hu et al., pp. 147–152, Palm Springs, Calif.

Yu, H.-S., B. V. Jackson, P. P. Hick, A. Buffington, T. K. Kim, N. V. Pogorelov, and C. C. Wu. (2013), The 3D reconstructed global solar wind boundary from remote-sensing IPS data, Space Weather Week, Boulder, Colo., 16–19 April. [Available at http://www.swpc.noaa.gov/sww/2014_SWW_Poster_Abstracts_Final.pdf.]

Zhao, X., and J. T. Hoeksema (1995), Prediction of the interplanetary magnetic field strength, *J. Geophys. Res.*, *100*, 19–33, doi:10.1029/94JA02266.